Volume 239, number 2, 351–357 FEB 06470 November 1988

A single-crystal EPR study of the reduced iron-quinone acceptor complex in reaction centers of *Rhodopseudomonas viridis*

R.G. Evelo, H.M. Nan and A.J. Hoff

Department of Biophysics, Huygens Laboratory of the State University, PO Box 9504, 2300 RA Leiden, The Netherlands

Received 12 September 1988

The EPR signal of the reduced iron-quinone complex in a single crystal of *Rhodopseudomonas viridis* has been investigated as a function of orientation. The results are consistent with $P4_32_12$ symmetry. Using the corresponding symmetry relations the directions of the principal axes of the effective g tensor of the iron-quinone complex were evaluated.

Photosynthesis; EPR; Iron-quinone acceptor; Single crystal; (*Rhodopseudomonas viridis*)

1. INTRODUCTION

Primary electron transport in bacterial photosynthetic reaction centers is initiated by photo-oxidation of the primary electron donor, a bacteriochlorophyll dimer (P) and the concomitant reduction of a primary acceptor, a quinone (Q_A) via a bacteriopheophytin (I). From Q_A the electron is transported to another quinone, Q_B. When singly reduced, both Q_A and Q_B are magnetically coupled to an Fe^{2+}:

$$PIQ_AFe^{2+}Q_B \xrightarrow{h\nu} P^*IQ_AFe^{2+}Q_B \longrightarrow$$
$$P^+I^-Q_AFe^{2+}Q_B \longrightarrow P^+IQ_A^-Fe^{2+}Q_B \longrightarrow$$
$$P^+IQ_AFe^{2+}Q_B^-$$

The role of this transition metal has been under investigation by a variety of experimental techniques such as Mössbauer, EXAFS, magnetic susceptibility and EPR spectroscopy [1–5], with which the electronic structure of the iron ion has been studied. It was concluded that the iron is in an Fe^{2+} high-spin ($S = 2$) state, which is independent of the oxidation state of the quinones. It is surrounded by six ligands that form a distorted octahedron [5]. The quinones are not directly liganded to the iron, although as noted above Q_A^- and Q_B^- have a magnetic interaction with Fe^{2+}. Extraction of Fe^{2+} and reconstitution of the RC with other divalent metals showed that Fe^{2+} is not necessary for $Q_A \longrightarrow Q_B$ electron transport [6]. The role of the iron has so far remained unclear.

Recent X-ray diffraction studies on single crystals of the RC complex of *Rhodopseudomonas viridis* and *Rhodobacter sphaeroides* R-26 have revealed the atomic structure of the RC with a resolution of 2.8 Å [7]. The X-ray data confirmed the above conclusions and provided the coordinates (± 0.26 Å) of the six ligands to the iron.

The availabilty of single crystals of RGs of *Rps. viridis* and *R. sphaeroides* makes it in principle possible to perform accurate orientational EPR studies of paramagnetic states of the RC, thus providing much more detailed information on electronic structure than possible with random samples. The first such studies were done on the oxidized primary donor P^+ [8] and on its triplet state P [9–11].

Here we report a study of the angular dependence of the EPR signal of the $PIQ_A^-Fe^{2+}$ state in a single crystal of *Rps. viridis*. We have estimated the position of the principal axes of the

Correspondence address: R.G. Evelo, Department of Biophysics, Huygens Laboratory of the State University, PO Box 9504, 2300 RA Leiden, The Netherlands

Published by Elsevier Science Publishers B.V. (Biomedical Division)
00145793/88/$3.50

crystal field tensor of the iron in the octahedron formed by its six ligands. This result should prove of value for the interpretation of the EPR signal of $Q_A^-Fe^{2+}$ in randomly oriented samples [5] and is a first step to obtain information on the electron distribution on the Fe^{2+} and its six ligands.

2. MATERIALS AND METHODS

Reaction centers (RCs) were prepared from *Rps. viridis* as described by Den Blanken and Hoff [12]. They were crystallized using a slightly modified method reported by Michel [13]. Crystals were grown by vapour diffusion in an aqeous solution of 20 mM Na_3PO_4 buffer solution, 3% (w/v) 1,2,3-heptanetriol, 0.3% LDAO and 4 M $(NH_4)_2SO_4$ and conserved in 20 mM Na_3PO_4 buffer solution, 1% 1,2,3-heptanetriol and 2.7 M $(NH_4)SO_4$. A crystal used for EPR experiments was first carefully transferred to a vial containing the storage solution to which 0.1 M sodium ascorbate and 40% glycerol had been added. The crystal was soaked for 10 min in this solution, after which it was mounted on a perspex rod and frozen under continuous illumination. This procedure generates the state $PIQ_A^-Fe^{2+}$ [14]. It is known that the crystals as grown by the above method do not contain Q_B [12,15]. The X-band (9 GHz) EPR spectra were recorded with a Varian E9 spectrometer equipped with an Oxford 900 He flow cryostat. All EPR experiments were performed in the dark at 5 K.

3. RESULTS AND DISCUSSION

EPR spectra have been observed of the iron-complexed Q_A^- in a single crystal of *Rps. viridis*. The crystal was first mounted with its *c*-axis (the long axis) vertical, and rotated around this axis in the fixed magnetic field. We observed sharp resonances with a linewidth of about 1.6 mT (fig.1). These resonances appear at $g = 1.81$ or 1.83. The crystal was then mounted with its *c*-axis horizontal and rotated around the vertical. Now almost no signal intensity was found; the maximum signal-to-noise ratio was about 2 for a very broad unstructured resonance.

In fig.2 the resonances found for rotation of the crystal about its *c*-axis are plotted as a function of the angle of the magnetic field in the *a,b* plane perpendicular to the *c*-axis. Only at very well defined angles (resolution $\pm 5°$) were resonances observed, which are represented by drawn and dashed lines in fig.2. The plot exhibits a 4-fold rotation symmetry. The directions corresponding to the maximum intensity at one particular *g* value ($g = 1.81$ or 1.83) consist of two identical sets of two perpendicular directions which are transformed into each other by a rotation of $\theta°$. Each set obeys the 4-fold (90°) rotation symmetry.

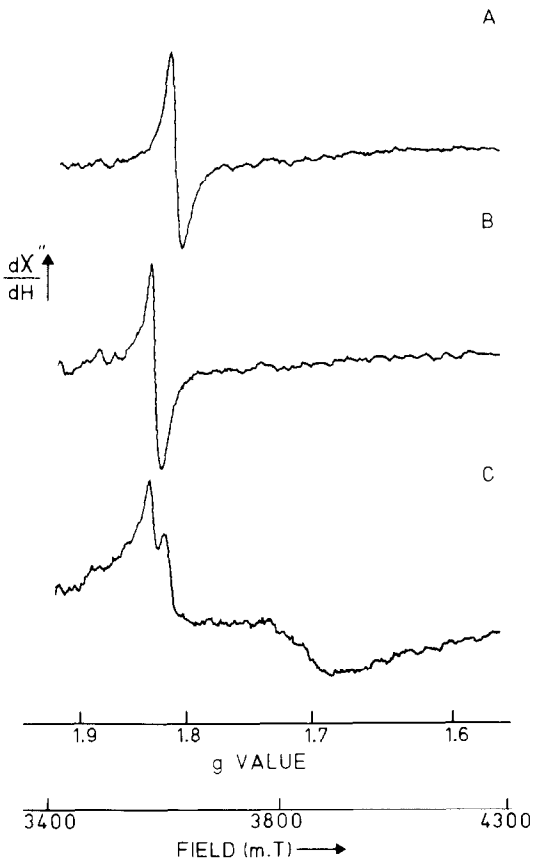

Fig.1. (A,B) EPR spectra of the iron-quinone complex in a single crystal of reaction centers of *Rps. viridis* with H_0 perpendicular to the *c*-axis. (C) EPR spectrum of a randomly frozen solution of *Rps. viridis* reaction centers. Temperature, 5.0 K; microwave frequency, 9.19 GHz; microwave power, 50 mW; modulation amplitude, 1.6 mT.

Deisenhofer et al. [16] have determined the space group of crystals of *Rps. viridis* with the same morphology as ours as $P4_32_12$ with four reaction centers in the asymmetric unit cell (eight in the symmetric unit cell). Applying the symmetry operations of the $P4_32_12$ symmetry group to an arbitrary direction in the *a,b* plane one recovers the symmetry relations of fig.2. We conclude therefore that our crystal has at least the $P4_32_12$ symmetry.

In a single crystal containing an anisotropic paramagnetic center one expects at arbitrary orien-

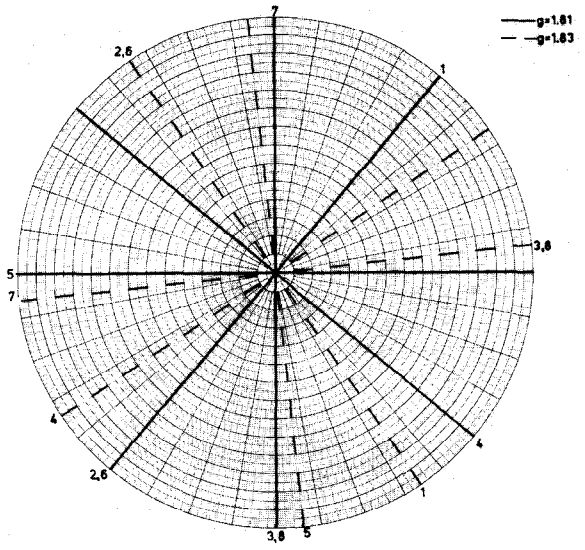

Fig.2. The relative orientations of the observed resonances as shown in fig.1A,B with H_0 perpendicular to the c-axis. (——) $g = 1.81$, (– – –) $g = 1.83$. Radial divisions are not used. The site assignment that is indicated at the rim corresponds to the columns headed O_1 and N_1 for the $g = 1.81$ and 1.83 lines, respectively.

tation for every non-equivalent site in the unit cell a single resonance line, that shifts when rotating the crystal. We have observed only small shifts over a rotation of 5–10°, the main effect of rotation being the disappearance of the sharp resonance (at either $g = 1.81$ or 1.83). We attribute this effect to small disorder of the crystal field and magnetic coupling tensors. We have observed similar effects in our investigation of the primary donor triplet state in a single crystal of *R. sphaeroides* R-26 [11], where outside their extremum positions, the resonance lines were severely broadened and, for some crystals, virtually disappeared. At and near the extremum position, the variation of resonance position with small angular variation is of course minimal. (At the extremum the derivative $dB/d\theta = 0$, where B is the resonance field and θ an orientation angle.) Apart from this, possibly quite small disorder, the crystals were well-ordered, giving narrow resonance lines at the extrema whose positions corresponded very well to those expected from the crystal symmetry [11]. For the present case, the situation is compounded by the fact that the resonance position is a function of both the crystal field and the magnetic coupling tensors (see below), which may be even more susceptible to small variations (perhaps <0.1 Å) in the atomic coordinates than the triplet fine structure parameters, so that the line broadening outside the extrema will be even more severe. We conclude, therefore, that the positions of the sharp resonances we observed (fig.2) reflect the extrema of the angular distribution function.

Since the crystal structure of *Rps. viridis* is very much like that of *R. sphaeroides* R-26 [17] the theoretical analysis of Butler et al. [5] should also apply to the EPR signal of the $Fe^{2+}Q^-$ complex in *Rps. viridis*. Briefly, Butler et al. [5] found that they could well simulate the $Fe^{2+}Q^-$ signal using a Hamiltonian that contained the crystal field tensors of the iron, with in addition an anisotropic magnetic interaction J, consisting of an isotropic exchange and an anisotropic (probably mostly dipolar) part. For simplicity all tensors were taken to be collinear, although for the dipolar interaction there is no reason that this need be so. Small angular variation between that tensor and the crystal field axes, however, did not make much difference in the simulations in [5].

The experimental resonance line shape of the randomly oriented $Fe^{2+}Q^-$ complex is, according to Butler et al. [5], made up of two contributions, one from a doublet ground state and one from a doublet excited state, whose intensities at 5 K are comparable. Each contribution has a rhombic line shape characterized by three field positions: two extrema (B_{1z},B_{1y} and B_{2z},B_{2y} for the ground and excited state, respectively) and two 'turning points', B_{1x} and B_{2x} at which the angular distribution function has a maximum. B_{1y} and B_{2y} lie far outside the field range of the present work and need not be considered further. B_{1z} and B_{2z} are the positions at which in the derivative ($d\chi''/dB$) representation of the resonance line two peaks occur: for *R. sphaeroides* R-26 at X-band at $g = 1.84$ and 1.68. The latter peak is very broad, and its position changes considerably with environmental conditions. At B_{1x} and B_{2x}, the $d\chi''/dB$ signal is at least an order less intense than at the B_{1z},B_{2z} positions, due to the much weaker curvature of the χ'' line shape at the former field positions. Thus, for randomly oriented RCs of *R. sphaeroides* R-26 one observes only the B_{1z} and B_{2z} peaks. From fig.1C we see that for *Rps. viridis* they correspond

to the g = 1.83 and 1.69 lines. Unlike *R. sphaeroides* R-26, the *Rps. viridis* line at g = 1.83 shows some structure with an additional smaller peak at g = 1.81, which apparently corresponds to the sharp resonance at g = 1.81 of the single crystal (fig.1A).

Turning now to the assignment of the sharp resonances of the single-crystal spectra, we can limit the possibilities considerably using the analysis of Butler et al. [5]. We are guided by the notion that the sharp lines reflect two of the B_{1x},B_{2x},B_{1z},B_{2z} extrema. First, we note that the g = 1.81 and 1.83 lines are never present at one and the same orientation. Thus, they cannot be due to the combinations B_{1x},B_{2x} or B_{1z},B_{2z}. Of the 8 other combinations possible, four more can be discarded because the B_{2z} position lies at g = 1.69, far from the g = 1.8 region. Taking, as demonstrated for *R. sphaeroides* R-26 [5], $J_y > 0$, we have $B_{1z} < B_{1x}$. We thus have to consider the three possible combinations: B_{1z},B_{2x}; B_{2x},B_{1z} and B_{1x},B_{1z} for the g = 1.83 and 1.81 lines in that order. The last combination is unlikely, as we would then in the single crystal observe only the ground doublet state whereas in the random solution the B_{2z} peak of the excited doublet state is clearly visible. It follows that we are left with the combinations B_{1z},B_{2x} or B_{2x},B_{1z} for the g = 1.83, 1.81 lines. Further discrimination is possible by considering the crystal symmetry, as shown below.

At this point one may ask why not all four extremum positions are observed when rotating the crystal. For the B_{2z} position it is likely that the line is very broad, since its position depends strongly on the value of the z component of the magnetic coupling J [5], which is expected to vary strongly with small orientational disorder. For the B_{1x} position we note that for the parameters used in table IIA of [5] the B_{1x} position depends a factor 4–5 stronger on the J_x component than the B_{2x} position, so that the same argument as used in [5] to explain the variation in the B_{2z} position as a function of environment probably applies to the B_{1x} position.

We will now consider the known atomic coordinates of the Fe atom and its ligands and the crystal symmetry discussed above, to attempt to assign further the sharp resonances to extremum positions corresponding to two particular principal axes of the crystal field tensor, and to estimate the orientation of the crystal field tensor in the crystal coordinate frame. The ligands form approximately an octahedron with the Fe atom in the center. To facilitate the discussion we label the His L190, His L230, His M217 and His M264 nitrogen ligands N_1, N_2, N_3 and N_4, respectively, and the two Glu M232 oxygens ligands, O_1 and O_2. By analogy to known crystal field tensors of Fe^{2+} complexes [18] we assume that the z-axis is pointing to one of the six octahedron tops. The x- and y-axes then lie in the base plane of the octahedron perpendicular to the z-axis but need not point to one of the ligands in this plane. We further assume that to a first approximation the aforementioned B_x,B_z positions correspond to the x and z principal axes of the crystal field tensor. We can now calculate the projection of the six iron ligand vectors on the a,b plane for all eight sites of the unit cell. If our assumption that the resonances observed for rotation of the magnetic field in the a,b plane are in directions close to the x,z principal axes is correct, then we must find that the calculated Fe-ligand projections obey the symmetry relations found experimentally (fig.2).

The calculated projections for each ligand i are found to give a symmetry pattern similar to that represented in fig.3 for the O_1 ligand, i.e. two sets

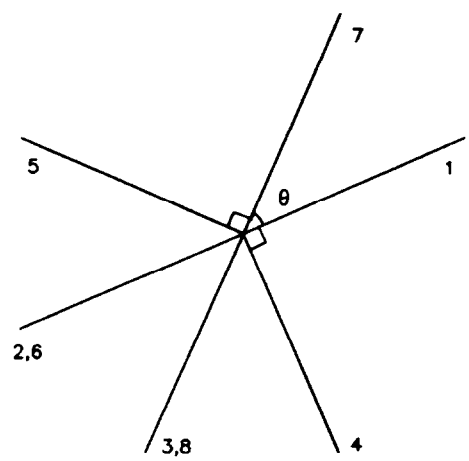

Fig.3. The calculated projections in the a,b plane of the Fe-O_1 directions for all eight sites.

of perpendicular directions that can be transformed into each other by a rotation over an angle θ. The angle θ_i for each ligand is listed in table 1. It is seen that the experimental angle for the $g = 1.81$ line, $\theta = 50.0°$, is close to the calculated angle $\theta = 43°$ for the O_1 ligand. This makes it likely that the Fe-O_1 vector coincides with one of the crystal field axes. To aid further in the assignment of the $g = 1.83$ and 1.81 lines, the angle between the projection in the a,b plane of a particular Fe-ligand vector relative to the projection of the Fe-O_1 vector for site 1 is shown for all eight sites and all six ligands in table 2. Note that the measured EPR transitions are invariant for a rotation over 180° (the polarity of the magnetic field does not affect EPR signals). This gives an ambiguity of 180° for the experimental angles of sites 4 and 5. From table 2 it is seen that only the angles for the projections of the Fe-N_1 and Fe-O_1 vectors agree with the experimental values for the $g = 1.83$ and 1.81 lines, respectively.

Table 1

Calculated angle θ defined as the angle between the two sets of perpendicular projections of the Fe ligands on the a,b plane and the experimental angles between the observed resonances defined in fig.2

Ligand	θ (°)	$g = 1.81$	$g = 1.83$
N_1	73		62.0
N_2	72		
N_3	70		
N_4	83		
O_1	43	50.0	
O_2	81		

Table 2

Calculated angles between the projection in the a,b plane for all the Fe ligand vectors relative to the projection of the Fe-O_1 vector of site 1

Site	N_1	N_2	N_3	N_4	O_1	O_2	$g = 1.83$	$g = 1.81$
1	105	212	213	20	0	298	106	0
2	285	32	33	200	180	118	288	180
3	32	285	284	117	137	199	42	140
4	195	302	303	110	90	28	196;16	90;270
5	122	15	14	207	227	289	134;314	230;50
6	285	32	33	200	180	118	281	180
7	212	105	104	297	317	19	229	320
8	32	285	284	117	137	199	42	140

The experimental and calculated angles are relative to the resonance $g = 1.81$ and the projection of the Fe-O_1 vector of site 1, respectively, which were both arbitrarily set to zero

From the above arguments it follows that in order to observe a sharp resonance when rotating the magnetic field in the crystallographic a,b plane, either the x or the z crystal field axis of a particular site must be close to the a,b plane (running through the Fe atom). The Fe-N_1 vector is the only ligand vector that makes a small angle with the a,b plane, viz. $\theta = 12.7°$. It is important to note that this angle is invariant to the symmetry operations of the $P4_32_12$ symmetry group, as are the angles of all other ligand vectors with the a,b plane. Since in all likelihood the crystal field z-axis lies along an iron-ligand vector, we therefore assign this axis to the Fe-N_1 direction. It follows that the $g = 1.83$ resonance represents the B_{1z} extremum position. The $g = 1.81$ resonance then represents the B_{2x} extremum position.

We have observed that the intensities of the sharp resonances decrease severely when the crystal is rotated in the a,b plane $\pm 5°$ away from the position at which the resonance has maximum intensity. Although the degree of broadening when rotating the crystal out of the a,b plane away from the 'maximum' positions may not be identical to that when rotating in this plane, it is nevertheless quite likely that neither the x- nor the z-axis may deviate more than 10–15° from the a,b plane for a sharp resonance to occur. As shown above this holds true for the z-axis when identifying it with the Fe-N_1 vector. We therfore conclude that the crystal field x-axis must also lie close to the a,b plane. Since it will also lie close to the $O_1N_2N_3N_4$ octahedron base plane, we may tentatively take the intersection of this base plane and the a,b plane to represent the crystal field x-axis. Note that the $O_1N_2N_3N_4$ 'plane' in reality is distorted; we have taken the $O_1N_2N_3$ plane, which is approximately perpendicular to the Fe-N_1 vector, to calculate the intersection with the a,b plane.

The results of our analysis are depicted in fig.4, which shows the ligand octahedron in the crystal a,b,c coordinate frame, and the x and z crystal field axes. Apparently, the more or less fortuitous positioning of one of the iron-ligand vectors close to the a,b plane, and the fact that one of the (approximate) base planes of the ligand octahedron lies almost perpendicular to the a,b plane allow the

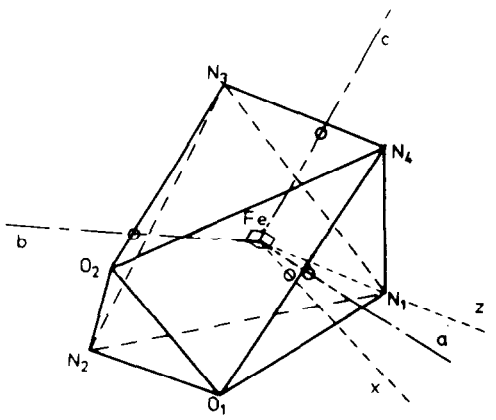

Fig.4. The distorted octahedron of the iron and its ligands according to the coordinates provided by Dr J. Deisenhofer. The crystallographic *a, b* and *c* axes are indicated. The *x* and *z* directions in the *a,b,c* coordinate frame are given by the relations (*x*): $-0.778a + 5.351b - 0.149c = 2.614Ac = 0$ and (*z*): $0.286a \pm 1.918b \pm 0.450c = 0\ A.\ a + b + a = -2.082$.

observation of two sets of sharp resonances when rotating the crystal around the vertical *c*-axis (perpendicular to the horizontal magnetic field). If the crystal is rotated around the vertical with its *c*-axis in the horizontal plane, the field will intersect the *a,b* plane in an arbitrary direction. As illustrated in fig.4 we then do not expect to see sharp resonances in the field region studied because at no angle does the field coincide with either the *x* or *z* crystal field. This agrees with our observations.

It is instructive to compare fig.4 with the results of table 2. In principle, for a perfect octahedron or an octahedron which is elongated (or compressed) along just one of the body diagonals (the *z*-axis), one would expect that the projection of all ligands in the base plane on a plane (here the *a,b* plane) through this body diagonal perpendicular to the base plane would show the same symmetry pattern, because the projections then overlap. Thus, one would then expect the columns in table 2 headed by N_2, N_3, N_4, O_1 to show approximately the same angle θ for any particular site, which would then correspond to the measured angle for that site. In reality from this set only column O_1 agrees with the experimental angles. This is a consequence of the fact that the base plane is quite distorted, as is apparent from fig.4. For a perfect octahedron, or elongated (compressed) octahedron, the difference between the angles in column N_1 (and column O_2) and those in column N_2, N_3, N_4 and O_1 should be $\pm 90°$. Table 2 shows that for these ligands the differential angles with column N_1 are ± 107, ± 108, ± 85 and $\pm 105°$, respectively, whereas the experimental difference is $\pm (96–108)°$ (fig.2). This means that none of the N_1, N_3, N_4 and O_1 ligand vectors is perpendicular to the Fe-N_1 vector, due to the distortion of the base plane. Furthermore, from the correspondence between the experimental differential angle and that found for the O_1 ligand, one can conclude that the plane through the Fe-O_1 vector and the *x*-axis of the crystal field tensor is more nearly perpendicular to the *z*-axis than that through the N_2, N_3, N_4 vectors and the *x*-axis. The experimental range (96–108)° (fig.2) indicates that the angle between the *z*-axis and the Fe-N_1 vector is about 6–18°, in agreement with that found between the Fe-N_1 vector and the crystallographic *a,b* plane.

The differential angle between columns O_2 and N_1 is $\pm 167°$, in contrast to the expected angle of 180° for a perfect octahedron, or an octahedron elongated or compressed along one of the body diagonals. This is a consequence of the non-collinearity of the Fe-N_1 and Fe-O_2 vectors (they make an angle of 153°). From the correspondence between the experimental positions and the calculated ones for the Fe-N_1 vector and the absence of such a correspondence for the Fe-O_2 vector (table 2), we conclude that the *z*-axis of the crystal field tensor lies closer to the Fe-N_1 vector than to the Fe-O_2 vector.

We may compare our results as shown in fig.4 with fig.4 of [19]. One then immediately observes that the $N_2N_3N_4O_1$ plane is one of the most undistorted planes in the octahedron. The Fe-ligand

Table 3

Fe-ligand distances calculated from the crystal coordinates (error ± 0.26)

Ligand	*R* (Å)
N_1	2.00
N_2	2.41
N_3	2.10
N_4	2.05
O_1	2.17
O_2	2.02

distances R calculated from the coordinates are shown in table 3. Although their differences fall within the error limit for the coordinates ($\pm$ 0.26 Å, therefore $\Delta R = \pm$ 0.19 Å), the Fe-N_1 and Fe-O_2 do seem to be the shortest ligands, making the ligand field of the iron ion that of a compressed octahedron.

Finally, we point out that our interpretation, viz. the $g = 1.83$ line represents the doublet ground state along the z crystal field axis and the $g = 1.81$ line the doublet excited state along the x-axis, may be tested by experiments at very low temperatures, where the excited state is frozen out, and at different microwave frequencies [5].

Acknowledgements: The authors wish to thank Dr J. Deisenhofer for sending the coordinates of the iron and its ligands in the *Rps. viridis* reaction center. This work was supported by the Netherlands Foundation for Chemical Research (SON) with financial aid from the Netherlands Organization for Scientific Research.

REFERENCES

[1] Butler, W.F., Johnston, D.C., Shore, H.B., Fredkin, D.R., Okamura, M.Y. and Feher, G. (1980) Biophys. J. 32, 967–992.
[2] Boso, B., Debrunner, P., Okamura, M.Y. and Feher, G. (1981) Biochim. Biophys. Acta 638, 173–177.
[3] Eisenberger, P., Okamura, M.Y. and Feher, G. (1982) Biophys. J. 37, 523–538.
[4] Bunker, G., Stern, E.A., Blankenship, R.E. and Parson, W.W. (1982) Biophys. J. 37, 539–551.
[5] Butler, W.F., Calvo, R., Fredkin, D.R., Isaacson, R.A., Okamura, M.Y. and Feher, G. (1984) Biophys. J. 45, 947–973.
[6] Debus, R.J., Feher, G. and Okamura, M.Y. (1986) Biochemistry 24, 2488–2500.
[7] Allen, J.P., Feher, G., Yeates, T.O., Komiya, H. and Rees, D.C. (1987) Proc. Natl. Acad. Sci. USA 84, 6162–6166.
[8] Allen, J.P. and Feher, G. (1984) Proc. Natl. Acad. Sci. USA 81, 4795–4799.
[9] Gast, P., Wasielewski, M.R., Schiffer, M. and Norris, J.R. (1983) Nature 305, 451–452.
[10] Gast, P. and Norris, J.R. (1983) FEBS Lett. 177, 277–280.
[11] Buma, W.J., Evelo, R.G., Groenen, E.J.J., Hoff, A.J., Nan, H.M. and Schmidt, J. (1987) Chem. Phys. Lett. 142, 231–236.
[12] Den Blanken, H.J. and Hoff, A.J. (1982) Biochim. Biophys. Acta 681, 365–374.
[13] Michel, H. (1982) J. Mol. Biol. 158, 567–572.
[14] Prince, R.C., Leigh, J.S. and Dutton, P.L. (1976) Biochim. Biophys. Acta 440, 622–636.
[15] Gast, P., Michalski, T.J., Hunt, J.E. and Norris, J.R. (1985) FEBS Lett. 179, 325–328.
[16] Deisenhofer, J., Epp, O., Miki, K., Huber, R. and Michel, H. (1984) J. Mol. Biol. 180, 385–398.
[17] Allen, J.P., Feher, G., Yeates, T.O., Rees, D.C., Deisenhofer, J., Michel, H. and Huber, R. (1986) Proc. Natl. Acad. Sci. USA 83, 8589–8593.
[18] Abragam, P. and Bleany, B. (1970) Electron Paramagnetic Resonance of Transition Ions, Clarendon, Oxford.
[19] Michel, H., Epp, O. and Deisenhofer, J. (1986) EMBO J. 10, 2445–2451.